Modelling, control and sensorless speed estimation of micro-wind turbines for deployment in Antarctica

Danilo X Llano*[1] and Richard A McMahon[2]

[1]Danilo X Llano was with the Electrical Engineering Division, University of Cambridge, 9 JJ Thomson Avenue CB3 0FA, Cambridge, UK. Now he is with WMG, University of Warwick, Coventry CV4 7AL, Coventry, UK
[2]WMG, University of Warwick, Coventry CV4 7AL, Coventry, UK
*dxl20@cantab.net

Abstract

This paper presents the modelling, control and sensorless speed estimation of two micro-wind turbines deployed by the British Antarctic Survey (BAS) in Antarctica. Mathematical models for the generators attached to an Ampair 100 and Rutland 913 wind turbines and their experimental validation are given. Also, a model for the wind turbines, particularly taking into account the power coefficient C_p versus tip speed ratio λ relationship was proposed and successfully evaluated on a wind turbine emulator test rig. This paper describes an analogue speed estimator board and a Kalman filter for estimating the shaft speed. These estimators use only DC side measurements to match the characteristics of the current version of the turbine control board. The wind turbine control and speed estimators were tested on the emulator test rig using real wind data from BAS research bases in Antarctica. Using only DC side measurements leads to low computation requirements to execute the algorithms in comparison to commonly used schemes that rely on AC measurements. In addition, the estimation algorithms are based on the model of a PM generator connected to a diode rectifier, as they can be used in a wider range of applications, including DC to DC converters with MPPT algorithms based on speed measurements.

1. Introduction

The Natural Environment Research Council (NERC) funds the British Antarctic Survey (BAS) to undertake or enable the majority of the UK's research in Antarctica. BAS relies heavily on micro-wind turbines to provide power to remote autonomous instruments in middle Antarctica where permanent human presence is impossible. The demands on these off-grid turbines are considerable: surviving high winds and low temperatures, relying on ice foundations, deployment by small aircraft and long periods between servicing opportunities (often greater than one year) [1, 2]. These demands have led BAS to develop its own controller electronics and algorithms for micro-wind turbines which are intended to optimise turbine survivability. BAS has tested different micro-wind turbine models in Antarctica, where devices from British manufacturers have proven to be well suited for this environment. At the same time, there have been larger scale wind energy

projects to power permanent manned research stations in Antarctica. For example, turbines at the Belgium Princess Elisabeth station produce about 10 kW on average, and the Australian Mawson station has about 300 kW installed capacity [3]. These large installations are located in the shores of Antarctica where the wind conditions are more moderate than in the middle of the continent.

Micro-wind turbines up to 0.3 kW, the type of device used to power remote data acquisition systems in Antarctica, are normally designed for battery charging, where low efficiency (especially at high wind speed) is tolerated in order to have a smooth output power versus wind speed curve. These turbines can be directly wired to a lead acid battery (not recommended by some manufacturers) but usually a charge regulator (boost/buck converter) is included to manage the charging cycle of the battery and prevent issues such as overcharging.

This present paper reports work on the modelling and control of micro-wind turbines for deployment in Antarctica, with its challenging wind conditions, thereby providing a valuable case study. In addition, there is a need for more effective energy harvesting and better condition monitoring in this application. Two micro-wind turbines currently used by BAS and rated at 100 W were considered: the Ampair 100 and the Rutland 913. Both models are designed for battery charging, with permanent magnet generators and built-in diode rectifiers. The research was divided into two main parts. The first part of this present study covers the modelling of the two micro-wind turbines, including details about their power coefficient and tip speed ratio curve and the PM generator attached to the wind turbine, with the aim of introducing a system level description of the devices and to confirm/complement data available from manufacturers. The second stage of this research was focused on control characterisation and sensorless speed estimation algorithms for micro-wind turbines using real wind data from Antarctica. However, the algorithms and conclusions drawn, are applicable to any other working environment.

A detailed model of the wind turbine and its generator is valuable to explain faults (failure analysis), prevent future damage (scheduled maintenance - a key action due to limited access to the stations) and to develop a more robust controller (predictive or advanced control) [4]. Micro-wind turbine modelling has been presented in several papers, particularly looking at mechanical aspects such as the effects of the blade design on the turbine aerodynamics [5, 6]. There are also papers reporting on power coefficient versus tip speed ratio curve measurements in wind tunnels [7, 8]. Those studies concentrated on the aerodynamics of the turbine and no significant details were given about the electrical generator itself.

The equipment already installed in Antarctica records variables such as wind speed and direction, temperature, input/output DC voltage and current; but there is also an interest in measuring the shaft speed of the turbine. An encoder could be included but it is bulky, expensive and likely to be unreliable in this harsh environment. A practical solution is adding a sensorless speed estimation algorithm based on electrical measurements. However, most schemes of sensorless estimation for motor drives or generators rely on AC current and voltage measurements [9, 10, 11]. This is not possible in the micro-wind turbines currently used by BAS since they have built-in diode rectifiers. The turbine is allowed to rotate around its hub and the DC power is transmitted to the battery charger via two brushes and slip rings. In this context, an analogue speed estimator or a sensorless estimation based only on DC side measurements would be ideal, although it will be less accurate compared to estimations using AC measurements.

The literature that refers to sensorless speed estimation based on DC variables is limited. In [12], DC voltage and current sensors are used to estimate the rotor position and speed to control a PM motor drive. In this paper, a simplified Kalman filter is proposed to estimate the shaft speed. This algorithm compensates for the uncertainty in machine parameters, non ideal power

electronics, and the fact that the BAS controller updates at about 23 Hz. The last condition is particularly challenging for the technique since the estimation cannot be updated frequently. This digital estimation technique is perfectly suitable for passive diode rectifiers and DC to DC controllers with MPPT algorithms based on speed tracking. The speed estimation is key for this last arrangement since the speed sensor is replaced by an estimation based on DC side measurements already available, leading to fewer moving components, more reliability and lower costs without significant hardware changes to the current electronic system. Additionally, an analogue approach to estimate the rotor speed from the frequency of DC voltage ripple is presented as an alternative solution. Both sensorless techniques, the Kalman filter and the analogue board, were trialled on the emulator test rig by using real wind data from Antarctica.

2. Emulator test rig

A wind turbine emulator test rig has been built to replicate the behaviour of a real wind turbine and also to characterize the electrical generators used in different micro-wind turbines [13, 14]. The prime mover is a servomotor rated at 3000 RPM, 19.2 Nm and 4.5 kW. It is controlled by an industrial drive and a target machine manufactured by Speedgoat that executes in real time a micro-wind turbine model in MATLAB/Simulink. A torque & speed transducer and an encoder were also included. Fig 1 shows the physical test rig.

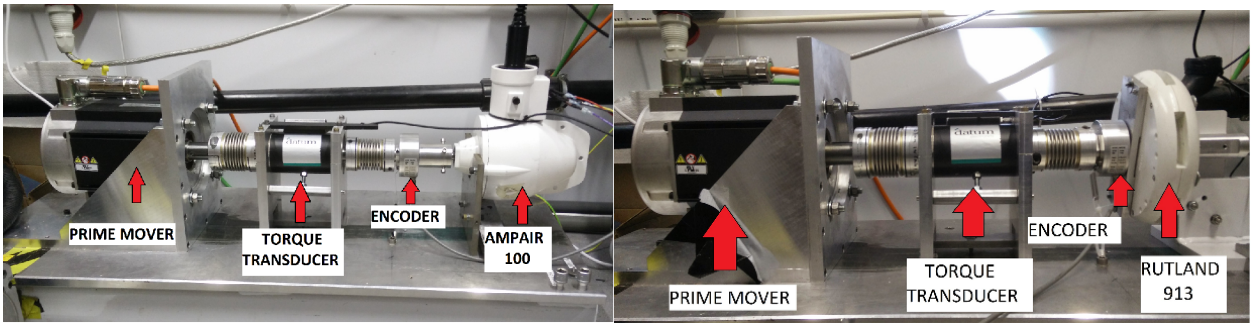

Fig. 1. *Test rig set up - Ampair turbine (left) and Rutland turbine (right)*

3. Generator modelling

The Ampair generator is a permanent magnet, two phase, radial flux generator while the Rutland is an axial flux, permanent magnet, three phase, star connected machine.

The generator modelling was done as follows: first at all, the phase resistances R_s, the L_d and L_q inductances, the emf constant and pole pairs were measured and are summarised in Table 1. Then, both generators were exercised by driving them at different speeds and AC loads. The model of the Ampair turbine is given in detail since this machine is unusually a two phase generator. The currents and voltages in the Ampair turbine were recorded and then compared with simulations in MATLAB/Simulink to validate the model.

Table 1 Machine parameters

Parameter	Ampair	Rutland
Phase resistance [Ω]	1.45	0.8
L_d inductance [mH]	23.7	1.31
L_q inductance [mH]	28.7	0.87
Pole pairs	3	4
Back emf constant [mVp/RPM]	51.5	45.2
Back emf constant (3rd harmonic) [mVp/RPM]	2.82	0
Back emf constant (5th harmonic) [mVp/RPM]	0.30	0

3.1. Ampair 100

Initial measurements showed that the emf voltage of this generator has noticeable harmonics to be considered in the modelling. The machine model can be directly written in the $\alpha\beta$ reference frame since both windings are physically 90 degrees shifted.

$$\begin{aligned}\frac{d}{dt}\begin{pmatrix} i_\alpha \\ i_\beta \end{pmatrix} &= Z^{-1}\begin{pmatrix} u_\alpha \\ u_\beta \end{pmatrix} - \phi P\omega_m Z^{-1}\begin{pmatrix} -\sin\theta \\ \cos\theta \end{pmatrix} - R_s Z^{-1}\begin{pmatrix} i_\alpha \\ i_\beta \end{pmatrix} \\ &\quad -2L_2 P\omega_m Z^{-1}\begin{pmatrix} \sin 2\theta & -\cos 2\theta \\ -\cos 2\theta & -\sin 2\theta \end{pmatrix}\begin{pmatrix} i_\alpha \\ i_\beta \end{pmatrix} - Z^{-1}P\omega_m \sum_{n=1}^{\infty}\gamma_n (2n+1)\begin{pmatrix} (-1)^{n+1}\sin(2n+1)\theta \\ \cos(2n+1)\theta \end{pmatrix}\end{aligned} \quad (1)$$

where ω_m is the shaft speed, P is the pole pairs, ϕ is the rotor flux, $i_{\alpha\beta}$ and $u_{\alpha\beta}$ are the current and voltage in the stator reference frame respectively, γ_n is the amplitude of the n^{th} harmonic and Z is defined in (2).

$$Z = \begin{pmatrix} L_1 - L_2\cos 2\theta & -L_2\sin 2\theta \\ -L_2\sin 2\theta & L_1 + L_2\cos 2\theta \end{pmatrix} \quad (2)$$

where $L_1 = \frac{1}{2}(L_q + L_d)$ and $L_2 = \frac{1}{2}(L_q - L_d)$. L_{dq} are the direct and quadrature inductances.

The Park transformation (3) was used to obtain the machine model in the dq reference frame in (4).

$$T = \begin{pmatrix} \cos\theta & \sin\theta \\ -\sin\theta & \cos\theta \end{pmatrix} \quad (3)$$

$$\begin{pmatrix} u_d \\ u_q \end{pmatrix} = \begin{pmatrix} L_d\frac{di_d}{dt} \\ L_q\frac{di_q}{dt} \end{pmatrix} + R_s\begin{pmatrix} i_d \\ i_q \end{pmatrix} + \begin{pmatrix} 0 \\ P\phi\omega \end{pmatrix} + \begin{pmatrix} -P\omega_m L_q i_q \\ P\omega_m L_d i_d \end{pmatrix} + P\omega_m\sum_{n=1}^{\infty}\Gamma_n \quad (4)$$

where Γ_n is defined in (5).

$$\Gamma_n = \begin{cases} (2n+1)\gamma_n\begin{pmatrix} \sin(2n+2)\theta \\ \cos(2n+2)\theta \end{pmatrix} & if\ n\ is\ odd \\ (2n+1)\gamma_n\begin{pmatrix} -\sin(2n)\theta \\ \cos(2n)\theta \end{pmatrix} & if\ n\ is\ even \end{cases} \quad (5)$$

Equation (6) describes the electromagnetic torque.

$$T_{em} = P\left(\lambda_d i_q - \lambda_q i_d\right) \tag{6}$$

where $\left[\begin{array}{cc} \lambda_d & \lambda_q \end{array}\right]^T$ is defined as

$$\left(\begin{array}{c} \lambda_d \\ \lambda_q \end{array}\right) = \left(\begin{array}{cc} L_d & 0 \\ 0 & L_q \end{array}\right)\left(\begin{array}{c} i_d \\ i_q \end{array}\right) + \phi\left(\begin{array}{c} 1 \\ 0 \end{array}\right) + \sum_{n=1}^{\infty}\Lambda_n \tag{7}$$

$$\Lambda_n = \begin{cases} \gamma_n \left(\begin{array}{c} -\cos\left(2n+2\right)\theta \\ \sin\left(2n+2\right)\theta \end{array}\right) & if\ n\ is\ odd \\ \gamma_n \left(\begin{array}{c} \cos\left(2n\right)\theta \\ \sin\left(2n\right)\theta \end{array}\right) & if\ n\ is\ even \end{cases} \tag{8}$$

Table 3 in the Appendix gives the voltage and current measurements and simulations for the Ampair generator at different speeds and AC loads. Light, medium and full load tests at various speeds were used to consider the entire operating range of the turbine. The errors are due to the fact that the generator phases were unbalanced and the values listed in Table 3 correspond to the average measurements of both phases, while the simulated model assumes the machine is balanced. The maximum error (9%) occurs for the simulated current at low speed and light load.

Measured and simulated voltage and current waveforms at 1.75 A and 500 RPM are plotted in Fig 2. The significant harmonic content in the waveforms was replicated by the model.

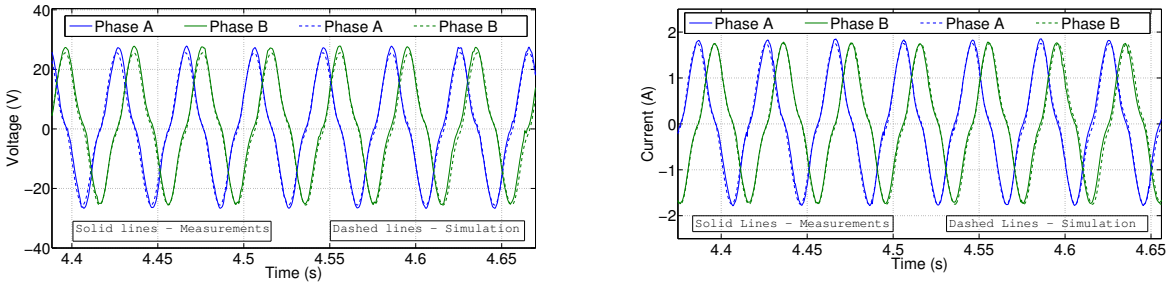

Fig. 2. *Measured and simulated voltage (left) and current (right) waveforms - Ampair turbine*

3.2. Rutland 913

The generator is an axial flux permanent magnet machine described by (9) and (10) in the dq reference frame [11]

$$u_d = R_s i_d + L_d\frac{di_d}{dt} - L_q i_q P\omega \tag{9}$$

$$u_q = R_s i_q + L_q\frac{di_q}{dt} + L_d i_d P\omega + P\omega\phi \tag{10}$$

The electromagnetic torque is presented in (11).

$$T_{em} = \frac{3}{2} P \left(\phi + \left(L_d - L_q \right) i_d \right) i_q \tag{11}$$

4. Wind turbine modelling

Micro-wind turbines can achieve relatively high rotational speeds (up to 1500 RPM) so that a PM generator with direct drive is the preferred configuration. Also, micro-wind turbines are designed to be as simple as possible without any active pitch or yaw control. They usually have a built-in diode bridge rectifier for connection to a battery or charge unit via brushes and slip rings.

The wind turbine model developed in this paper is based on the work done in [13, 14] for small-wind turbines with different mechanical parameters (blade radius, turbine inertia), and performance parameters (tip speed ratio, power coefficient). The tip speed ratio and power coefficient are two key values to model a wind turbine due to its performance and dynamics are strongly tied to both parameters. The tip speed ratio (λ) is defined in (12)

$$\lambda = \frac{\omega_m R_b}{v} \tag{12}$$

where ω_m is the rotational speed of the turbine, R_b is the blade radius and v is the wind speed.

The power output P_{out} of a wind turbine can be written as follows:

$$P_{out} = \frac{1}{2} C_p \rho \pi R_b^2 v^3 \tag{13}$$

where ρ is the air density, R_b is the blade radius, v is the wind speed and C_p is the power coefficient of the turbine [13].

In the literature [15, 16, 17, 18], the relationship between the tip speed ratio (λ), wind direction (β) and the power coefficient (C_p) is usually given as:

$$C_p = \alpha_1 \left(\frac{\alpha_2}{\lambda_i} - \alpha_3 - \alpha_5 \beta \right) e^{-\alpha_4 / \lambda_i} \tag{14}$$

where α_n is a parameter to be estimated and

$$\frac{1}{\lambda_i} = \frac{1}{\lambda + 0.08\beta} - \frac{0.035}{\beta^3 + 1} \tag{15}$$

Micro-wind turbines are free to align themselves with the wind direction, therefore it is reasonable to assume $\beta = 0$. The power coefficient waveform has a maximum at the optimal tip speed ratio so that the following equation can be written

$$C_{pmax} = \alpha_1 \left(\frac{\alpha_2}{\lambda_{opt}} - \alpha_3 \right) e^{-\alpha_4 / \lambda_{opt}} \tag{16}$$

Also, at the maximum point $\frac{dC_p}{d\lambda} = 0$ and

$$-\alpha_2 + \frac{\alpha_2\alpha_4}{\lambda_i} - \alpha_3\alpha_4 \;\; = \;\; 0 \tag{17}$$

Equations (16) and (17) were solved in MATLAB (fsolve routine) for different C_{pmax} and λ_{opt} to get α_n for each turbine. After various trials, the parameters were estimated as $C_{pmax} = 0.30$, $\lambda_{opt} = 2.5$ and $C_{pmax} = 0.25$, $\lambda_{opt} = 3.75$ for the Ampair and Rutland turbine respectively. Table 4 in the Appendix summarises the power output, power coefficient and tip speed ratio at different wind speeds from the datasheet, simulation and experimental implementation for the Ampair turbine. A buck converter was used to maintain the output voltage at 15 V. Similarly, Table 5 in the Appendix presents the corresponding results for the Rutland turbine. It can be seen that there is a good agreement between simulation and experimental results, but there is a more significant difference with the datasheet values, particularly at low wind speeds. Unfortunately, no details are given by the manufacturers about their testing conditions to obtain the power versus wind speed curve. Also, the wind turbine model used in this paper assumes that the optimal tip speed ratio and optimal power coefficient are constant throughout the different wind speeds. This is a good assumption for system level simulations but detailed wind tunnel measurements highlighted that the optimal tip speed ratio and optimal power coefficient change with the wind speed [19, 20]. This is the main reason for the different between simulation and measurement results, even though the difference is smaller compared to the datasheet values.

5. BAS Turbine Controller

The turbine controller developed by BAS is used for both turbines and has the following structure:

1. The input power to the board comes from the built-in passive diode rectifier in the wind turbine.

2. A PWM controlled MOSFET across the DC line limits the DC voltage and current [21]. The maximum values at the final output are 18 V and 5 A with 0.5 V and 0.5 A hysteresis bands respectively. The input current is limited to 12 A (average) and 15 A (peak). In case the output current and/or voltage exceed their maximum values the PWM controlled MOSFET short-circuits the diode rectifier output to slow down the generator and limit the power output. The PWM switching frequency is 18 kHz and the duty cycle is updated at 23 Hz. When the variables are within range the switching MOSFET is off (bypass operation).

3. A last resort MOSFET is included as a clamp in case the output voltage exceeds 20 V. This second MOSFET connects a dump resistor across the diode bridge terminals. Input/output currents and voltages are measured in this board [2].

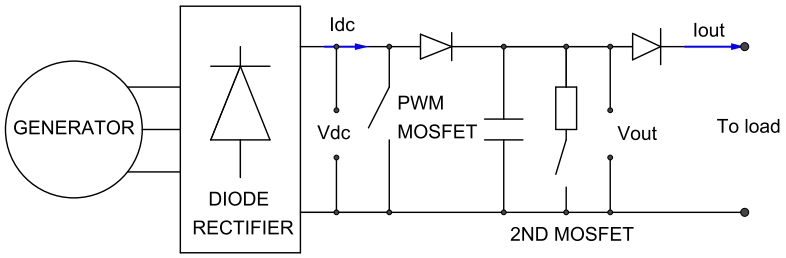

Fig. 3. *BAS controller scheme*

6. Sensorless speed estimation

A simplified Kalman filter is proposed to estimate the shaft speed without any physical change in the controller described in the previous section. The Kalman algorithm compensates for uncertainty in parameters, modelling approximations and noise. The estimation is based only on DC measurements, with reduced computation requirements and is executed at 23 Hz.

The Kalman filter algorithm is detailed in Algorithm 1. Notation $\Gamma\left[n\,|m\right]$ in Algorithm 1 means the value of the matrix Γ at instant n taking into account m previous updates. In this particular application, the function $f(x(k),u(k),k)$ is a vector which describes the relationship between the shaft speed and the DC current and voltage.

Algorithm 1 Extended Kalman Filter [11, 22]

$$
\begin{aligned}
X\left[k|k-1\right] &= f(x(k),u(k),k) \\
P\left[k|k-1\right] &= \Phi[k-1]P[k-1|k-1]\Phi^{T}[k-1]+Q\left[k-1\right] \\
K\left[k\right] &= P[k|k-1]\overline{H}^{T}[k]\cdot\left(\overline{H}[k]P[k|k-1]\overline{H}^{T}[k]+R[k]\right)^{-1} \\
X\left[k|k\right] &= X\left[k|k-1\right]+K[k]\left(Y[k]-\overline{H}[k]X[k|k-1]\right) \\
P[k|k] &= P[k|k-1]-K[k]\overline{H}[k]P[k|k-1]
\end{aligned}
$$

where Φ is defined as:

$$
\Phi \approx \left.\frac{\partial f\left(x(k),u(k),k\right)}{\partial x}\right|_{X(k|k)}
$$

The estimation scheme is shown in Fig 4.

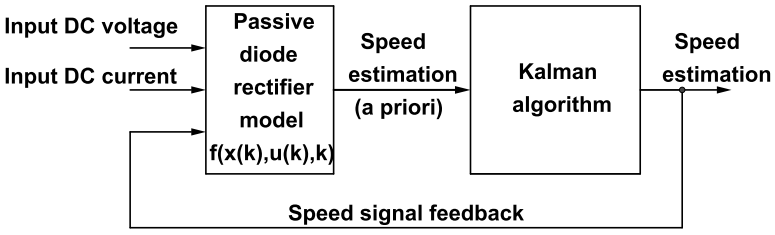

Fig. 4. *Speed estimation scheme*

The two generators with different configurations (two and three phase) were used to demonstrate the applicability of this technique to a wide range of electrical machines. The core algorithm is the same, the only difference is the mathematical relationship between the shaft speed and the DC voltage and current described by the function $f(x(k), u(k), k)$. The proposed speed estimation is well suited for passive diode rectifiers, but essential for DC to DC converters performing maximum power point tracking (MPPT) algorithms based on speed, as the techniques described in [23].

The following describes the mathematical derivation of the function $f(x(k), u(k), k)$ for two and three phase PM generators and the corresponding experimental results.

6.1. Ampair 100 (two phase)

The emf of this turbine can be written as

$$V_a = \sqrt{2}V_s \sin \omega t + \sum_{k=1}^{\infty} \gamma_k \sin\left(2k+1\right)\omega t \tag{18}$$

where V_s is the rms value of the main harmonic, γ_k is the amplitude of the k-th harmonic and ω is the electrical angular frequency.

The voltage after the diode rectifier is given by

$$V_{do} = \frac{4}{\pi}V_s + \frac{4}{\pi}\sum_{k=1}^{\infty} \gamma_k \frac{1}{2n+1} \sin\left(\left(2n+1\right)\frac{\pi}{4}\right) \tag{19}$$

Using the approximate method in [24] to estimate the effect of the phase inductance and resistance on the DC voltage it is possible to write (20). It is assumed that each diode bridge rectifier provides half of the total DC current I_{dc}.

$$V_{dc} = \frac{4}{\pi}V_s + \frac{4}{\pi}\sum_{k=1}^{\infty} \gamma_k \frac{1}{2n+1} \sin\left(\left(2n+1\right)\frac{\pi}{4}\right) - \frac{P\omega_m}{\pi}L_s I_{dc} - \frac{1}{2}R_s I_{dc} \tag{20}$$

where V_{dc} is the DC voltage, I_{dc} is the DC current, V_s is the back emf rms value of the fundamental, γ_n is the amplitude of the n^{th} harmonic, P is the pole pairs, ω_m is the rotor speed, R_s and L_s are the phase resistance and inductance respectively. The phase inductance is defined as follows:

$$L_s \;=\; L_1 \pm L_2 \cos 2\theta \tag{21}$$

where $L_1 = \frac{1}{2}(L_q + L_d)$and $L_2 = \frac{1}{2}(L_q - L_d)$.

However, L_d and L_q are almost the same and $L_1 \gg L_2$ so that it is possible to approximate and simplify the calculations by taking $L_s \approx L_1 = \frac{1}{2}(L_d + L_q)$

Finally, in a PM generator the emf for each harmonic is proportional to the speed

$$V_s = k_v \omega_m \qquad \gamma_n = (2n+1)\, k_{vn} \omega_m \tag{22}$$

Equation (23) is solved from (20) and (22) and estimates the rotational speed. Only DC measurements are required.

$$\omega_m \;=\; \frac{\pi}{4}\left(\frac{V_{dc} + \frac{1}{2}R_s I_{dc}}{k_v + \sum_{n=1}^{\infty} k_{vn} \sin\left((2n+1)\frac{\pi}{4}\right) - \frac{1}{4}P L_s I_{dc}}\right) \tag{23}$$

Whilst equation (23) can be used to estimate the rotor speed, a more robust algorithm is needed to compensate for uncertainty in parameters and the low updating frequency (23 Hz).

Equation (23) can be rewritten as

$$V_{dc} \;=\; \psi_1 \omega_m - \psi_2 \omega_m I_{dc} - \psi_3 I_{dc} \tag{24}$$

where $\psi_1 = \frac{4}{\pi}\left(k_v + \sum_{n=1}^{\infty} k_{vn} \sin\left((2n+1)\frac{\pi}{4}\right)\right)$, $\psi_2 = \frac{P}{\pi} L_s$ and $\psi_3 = 0.5 R_s$

However, when the controller is active, the input voltage is chopped and its mean value behaves as the voltage in a boost converter. The controller calculates a variable PWM duty cycle D depending on the working conditions. To account for this switching operation mode, the input voltage V_{dc} and current I_{dc} measurements are scaled by $\frac{1}{1-D}$ and $1 - D$ respectively. $\frac{1}{1-D}$ is the conversion ratio of an ideal boost converter. The Kalman algorithm compensates for approximations made in the model. If $D = 0$ the scaling factors are 1.

$$V_{dc}^* = \frac{1}{1-D} V_{dc} \qquad I_{dc}^* = (1-D)\, I_{dc} \tag{25}$$

A state space system ((26) to (29)) was defined to use the Kalman filter algorithm to estimate the shaft speed. The system is simple and involves mostly scalar operations.

$$f\left(x(k), u(k)\right) \;=\; \begin{pmatrix} \psi_1 \omega_m[k] - \psi_2 \omega_m[k]\, I_{dc}^*[k] - \psi_3 I_{dc}^*[k] \\ \omega_m[k] \end{pmatrix} \tag{26}$$

$$x[k] \;=\; \begin{bmatrix} V_{dc}^*[k] & \omega_m[k] \end{bmatrix}^T \tag{27}$$

$$u[k] = I_{dc}^* \qquad H[k] = \begin{bmatrix} 1 & 0 \end{bmatrix} \tag{28}$$

$$\Phi = \begin{bmatrix} 0 & \psi_1 - \psi_2 I_{dc}^* \\ 0 & 1 \end{bmatrix} \tag{29}$$

The algorithm was evaluated using the real wind speed profile (from the Halley VI station in Antarctica) plotted in Fig 5 (left). This profile rapidly rises from 4 m/s to 12 m/s. The controller described in Section 5 was used with the emulator test rig for sensorless speed estimation. Fig 5 (right) shows the estimated and measured speed for the Ampair turbine. Both signals match well.

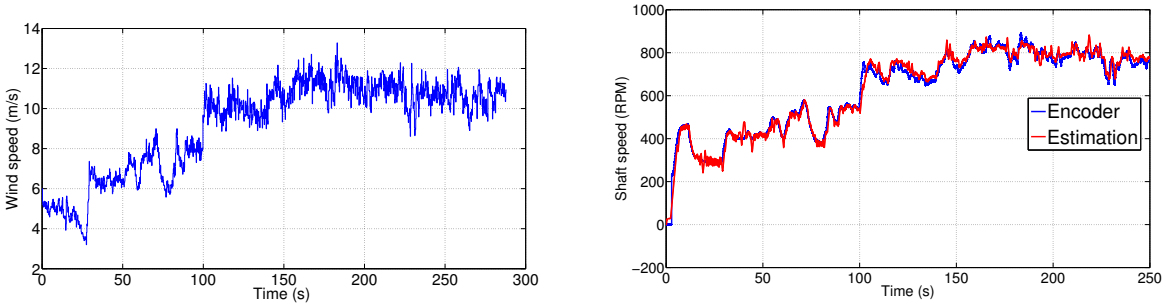

Fig. 5. *Wind speed profile (left) and sensorless estimation - Ampair turbine (right)*

6.2. Rutland 913 (three phase)

The same estimation algorithm used for the Ampair turbine was applied to the Rutland turbine, but different expressions for the DC voltage and shaft speed were required. Equations (20) and (23) were replaced by (30) and (32) respectively.

$$V_{dc} = \frac{3\sqrt{2}E_{ab}}{\pi} - \frac{3P\omega_m}{\pi} L_s I_d - 2R_s I_{dc} \tag{30}$$

where V_{dc} is the DC voltage, I_{dc} is the DC current, E_{ab} is the emf rms value, P is pole pairs, ω_m is the rotor speed, R_s and L_s are the phase resistance and inductance respectively. To simplify L_s was again taken as $\frac{Ld+Lq}{2}$.

In a PM generator the emf rms value is proportional to the speed

$$E_{ab} = k_v \omega_m \tag{31}$$

Equation (32) estimates the rotational speed and it was obtained from (30) and (31). Again, it should be observed that only DC measurements are required.

$$\omega_m = \frac{\pi}{3}\left(\frac{V_{dc} + 2R_s I_{dc}}{\sqrt{2}k_v - PL_s I_{dc}}\right) \tag{32}$$

Equation (32) can be rewritten as

$$V_{dc} = \psi_1 \omega_m - \psi_2 \omega_m I_{dc} - \psi_3 I_{dc} \tag{33}$$

where $\psi_1 = \frac{3}{\pi}\sqrt{2}k_v$, $\psi_2 = \frac{3P}{\pi}L_s$ and $\psi_3 = 2R_s$

As in the previous sub-section, the input voltage and current were compensated by the factors $\frac{1}{1-D}$ and $1 - D$ respectively. Also, equations (26) - (29) were used in the estimation algorithm for the Rutland turbine, but with the definitions in (32) and (33).

The wind speed profile in Fig 5 (left) was used again to test the sensorless speed estimation algorithm for the Rutland turbine. Fig 6 shows the estimated and measured speed for the Rutland turbine. The estimated signal tracks the measured speed properly.

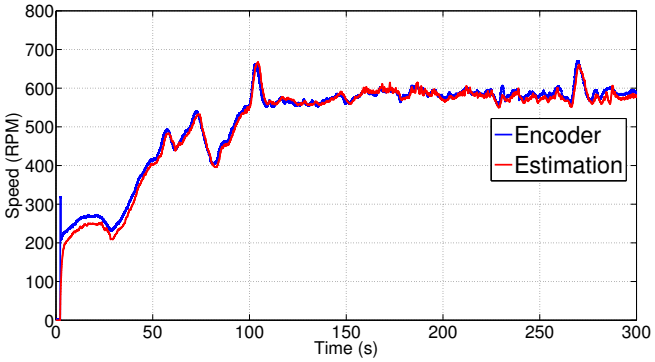

Fig. 6. *Sensorless estimation - Rutland*

6.3. Observability of the estimator

The Observability establishes if the system variables can be estimated from measurements, but does not imply anything about the quality or accuracy of the estimations. This system characteristic is useful for identifying working conditions where an estimator could fail. The observability matrix for this estimator is defined in (34) according to the guidelines given in [25, 26].

$$O = \begin{pmatrix} \nabla \left(H\left[k\right] x\left[k\right] \right) \\ \nabla \left(\nabla H\left[k\right] x\left[k\right] \right) \cdot f\left(x\left(k\right), u\left(k\right) \right) \end{pmatrix} \tag{34}$$

with $H\left[k\right] = \begin{bmatrix} 1 & 0 \end{bmatrix}$, $x\left[k\right] = \begin{bmatrix} V_{dc}^{*}\left[k\right] & \omega_m\left[k\right] \end{bmatrix}^T$ and $f\left(x\left(k\right), u\left(k\right) \right)$ as defined in (26). The system is observable if $rank\left(O\right) = n$, where n is the number of state space variables.

Using the definitions already stated for this system:

$$O = \begin{pmatrix} 1 & 0 \\ 0 & \psi_1 - \psi_2 I_{dc}^{*} \end{pmatrix} \tag{35}$$

and $n = 2$. It is obvious that the system is observable except for $I_{dcCRITICAL}^{*} = \frac{\psi_1}{\psi_2}$. The critical current was calculated with the parameters in Table 1 and definitions in (24) and (33). $I_{dcCRITICAL}^{*}$ was 18.56 A and 98.97 A in the Ampair and Rutland turbine respectively. The critical current in the Rutland turbine is significantly out of its practical operation range since the power rating of the device is 100 W and 12 V. For the Ampair turbine, the critical current is almost double the rated current at 12 V and 100 W.

6.4. Analogue board for speed estimation

An analogue approach to estimate the rotor speed from the frequency of the DC voltage ripple was also developed. This approach was originally proposed in the BAS control board but never implemented successfully. The board uses a frequency to voltage conversion chip by Texas Instruments (LM2917-8) followed by an active band pass filter to eliminate the DC component from the input voltage, some of the medium range frequencies associated with the unbalanced phases in the

generator, and also higher frequencies related to the switching controller, and electrical noise. The frequency to voltage conversion chip is essentially a zero crossing detector, therefore attenuation of unwanted frequencies is key to prevent false detections. Fig 7 shows the block diagram of the board and its physical realisation.

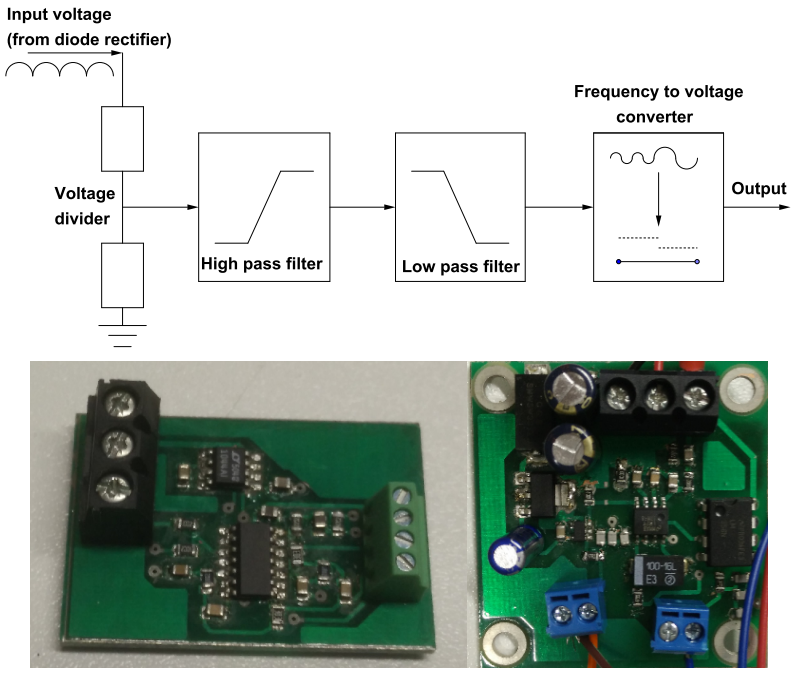

Fig. 7. *Analog speed estimation scheme (top), filter board (left bottom) and frequency to voltage board (right bottom)*

In an ideal three phase generator all the phases are balanced and the first frequency component of the DC voltage ripple is six times the fundamental frequency. However, initial measurements highlighted that the Rutland generator was not properly balanced as shown in Fig 8 (left). It can be observed that the actual voltage ripple is twice the fundamental frequency. The Rutland turbine is expected to operate between 200 and 1500 RPM which translates to an electrical frequency of 15 to 100 Hz. Considering that the main frequency component of the voltage ripple is twice the electrical frequency, then the frequency of the voltage ripple would be between 30 and 200 Hz. Consequently, the band pass filter was designed to filter out frequencies less than 7 Hz and greater than 220 Hz. The Sallen-Key topology was used to implement the filters (2nd order high pass filter and 4th order low pass filter).

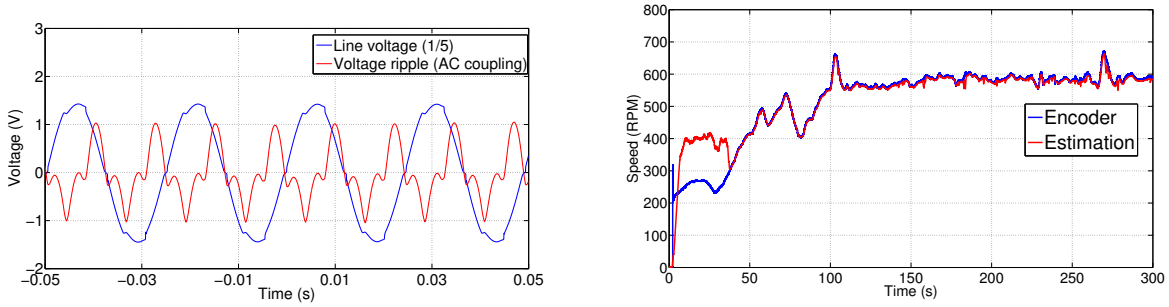

Fig. 8. *Voltage ripple waveform (left) and Speed estimation with analog board - Rutland (right)*

The board was tested with the Rutland turbine, but the same hardware can be used with the Ampair turbine as well. The only difference is the later signal processing.

Fig 8 (right) shows the speed estimation for the Rutland turbine using the frequency to voltage board and the wind speed profile in Fig 5. There estimation was accurate and reliable at medium and high speeds, but it can be seen that the board was not able to track speeds under 300 RPM. Below this speed the low pass filter was not able to filter out unwanted frequencies associated with the unbalanced generator and the board overestimated the actual frequency by detecting too many zero crossing points. According to the turbine manufacturer, the cut-in speed of the Rutland turbine is 2.5 m/s (minimum speed of about 240 RPM) [27]. Therefore, this analogue board still works well over most of the expected operating range.

The mean absolute error (MAE) and the maximum estimation error have been calculated for both estimation techniques, Kalman filter and analogue board using the following equation.

$$MAE = \frac{1}{n}\sum_{i=1}^{n}|y_i - \hat{y}_i|$$

where n is the number of samples, y_i is the measured variable and $\hat{y}_i$ is the estimated variable

Table 2 Error in estimations (in RPM)

	Ampair (Kalman)	Rutland (Kalman)	Rutland (Analogue)
MAE	9.45	8.46	12.88
Max error	126	63	149

Table 2 shows the MAE and the maximum estimation error in all the cases. It can be seen that the Kalman filter has better performance. The maximum error occurs immediately after the turbine start-up and it is due to the convergence time of the filter. Similarly, the MAE is largely influenced by the difference between the measured and estimated signals at the start-up and low speed. Once the Kalman filter converges, the difference between the estimated and measure signal is minimal. According to the manufacturers' data, the cut-in speed for both turbines is around 240 RPM, in which case the estimators can cover most of the operating range.

7. Conclusions

This paper has presented a system level study of micro-wind turbines, looking at their modelling, control and instrumentation. Two micro-wind turbines were studied in detail: the Ampair 100

and the Rutland 913. Models for the electrical generator itself and the power coefficient versus tip speed ratio curve were proposed and validated with simulations in MATLAB/Simulink and experiments on an emulator test rig. Afterwards, a digital speed estimation technique based on a Kalman filter was developed and successfully tested in two and three phase generators by using real wind data from Antarctica and the turbine controller designed by BAS. The novelty of this digital estimation technique is that only DC side measurements are required leading to low computation requirements to execute the algorithms in comparison to commonly used schemes that rely on AC measurements. This digital technique does not depend on the DC to DC converter used in the controller or the ripple of the DC measurements and works properly over a wide range of operating conditions. Later on, a frequency to voltage conversion board was designed to estimate the shaft speed from the frequency of the DC voltage ripple. All the estimation algorithms, digital and analogue, were successfully tested and can be implemented in similar turbines working in any other environment. The digital technique is the preferred solution because it does not require extra hardware and worked properly over the entire range of operating speeds. Applications in Antarctica were particularly interesting because of their harsh working conditions that challenge the control characterisation and estimation algorithms, and the availability of detailed data about the wind conditions. However, the controller and estimation routines proposed in this present paper can be implemented in a wider range of wind energy applications. The core algorithm and equations in the Kalman filter are based on the model of a PM generator (two or three phase) connected to passive diode rectifier and this arrangement is indeed one of the most commonly used configuration in micro and small-scale wind turbines up to 5 kW.

8. Acknowledgements

This research was supported by the Semiconductor Research Corporation (SRC) and the Texas Analog Center of Excellence (TxACE) through the Task ID: 1836.069, Electronic Systems for Small Wind Turbines and NERC IAA Knowledge Exchange Awards in collaboration with the British Antarctic Survey (BAS)

9. References

[1] T. Tin, B. Sovacool, and D. Blake, "Energy efficiency and renewable energy under extreme conditions: Case studies from Antarctica," *Renewable Energy*, vol. xxx, pp. 1–9, 2009.

[2] M. C. Rose, "Variable speed wind generator control in Antarctica," *Geophysical Research Abstracts*, vol. 9, p. 02051, 2007.

[3] C. McKenzie, K. Stephen, Z. Xin, M. Wagner, and D. Wainwright, "Windmills in Antarctica," University of Canterbury, Tech. Rep., 2010.

[4] Z. Hameed, Y. Hong, Y. Cho, S. Ahn, and C. Song, "Condition monitoring and fault detection of wind turbines and related algorithms: A review," *Renewable and Sustainable Energy Reviews*, vol. 13, no. 1, pp. 1 – 39, 2009. [Online]. Available: http://www.sciencedirect.com/science/article/pii/S1364032107001098

[5] F. Wang, L. Bai, J. Fletcher, J. Whiteford, and D. Cullen, "The methodology for aerodynamic study on a small domestic wind turbine with scoop," *Journal of Wind Engineering*

and Industrial Aerodynamics, vol. 96, no. 1, pp. 1 – 24, 2008. [Online]. Available: http://www.sciencedirect.com/science/article/pii/S0167610507000797

[6] F. Campagnolo, "Wind tunnel testing of scaled wind turbine models: Aerodynamics and Beyond," Ph.D. dissertation, Politecnico di Milano, 2013.

[7] T. Chen and L. Liou, "Blockage corrections in wind tunnel tests of small horizontal-axis wind turbines," *Experimental Thermal and Fluid Science*, vol. 35, no. 3, pp. 565 – 569, 2011. [Online]. Available: http://www.sciencedirect.com/science/article/pii/S0894177710002438

[8] G. Comyn, D. Nobes, and B. Fleck, "Performance evaluation and wake study of a micro wind turbine," *Transactions of the Canadian Society for Mechanical Engineering*, vol. 35, no. 1, pp. 101–117, 2011.

[9] P. Acarnley and J. Watson, "Review of position-sensorless operation of brushless permanent-magnet machines," *Industrial Electronics, IEEE Transactions on*, vol. 53, no. 2, pp. 352–362, April 2006.

[10] W. Qiao, X. Yang, and X. Gong, "Wind Speed and Rotor Position Sensorless Control for Direct-Drive PMG Wind Turbines," *Industry Applications, IEEE Transactions on*, vol. 48, no. 1, pp. 3–11, Jan 2012.

[11] P. Vas, *Sensorless vector and direct torque control*, ser. Monographs in electrical and electronic engineering. Oxford University Press, 1998.

[12] A. Piippo, K. Suomela, M. Hinkkanen, and J. Luomi, "Sensorless PMSM Drive with DC-link Current Measurement," in *Industry Applications Conference, 2007. 42nd IAS Annual Meeting. Conference Record of the 2007 IEEE*, Sept 2007, pp. 2371–2377.

[13] M. Tatlow, "Wind Turbine Emulator System for Testing Small-Scale Wind Generators and Associated Power Electronics," Master's thesis, University of Cambridge, 2011.

[14] D. Llano, M. Tatlow, and R. McMahon, "Control algorithms for permanent magnet generators evaluated on a wind turbine emulator test-rig," in *Power Electronics, Machines and Drives (PEMD 2014), 7th IET International Conference on*, April 2014, pp. 1–7.

[15] J. Slootweg, S. de Haan, H. Polinder, and W. Kling, "General model for representing variable speed wind turbines in power system dynamics simulations," *Power Systems, IEEE Transactions on*, vol. 18, no. 1, pp. 144–151, Feb 2003.

[16] O. Wasynczuk, D. Man, and J. Sullivan, "Dynamic Behavior of a Class of Wind Turbine Generators During Randon Wind Fluctuations," *Power Apparatus and Systems, IEEE Transactions on*, vol. PAS-100, no. 6, pp. 2837–2845, June 1981.

[17] J. De Kooning, L. Gevaert, J. Van de Vyver, T. Vandoorn, and L. Vandevelde, "Online estimation of the power coefficient versus tip-speed ratio curve of wind turbines," in *Industrial Electronics Society, IECON 2013 - 39th Annual Conference of the IEEE*, Nov 2013, pp. 1792–1797.

[18] S. M. Muyeen, J. Tamura, and T. Murata, *Stability Augmentation of a Grid-connected Wind Farm*. Springer, 2009.

[19] D. X. Llano and R. A. McMahon, "Control techniques with system efficiency comparison for microwind turbines," *IEEE Transactions on Sustainable Energy*, vol. 8, no. 4, pp. 1609–1617, Oct 2017.

[20] D. Llano, "Sensorless control techniques and associated power electronics for generators in micro and small-scale wind turbines," Ph.D. dissertation, University of Cambridge, 2016.

[21] D. Whaley, W. Soong, and N. Ertugrul, "Investigation of switched-mode rectifier for control of small-scale wind turbines," in *Industry Applications Conference, 2005. Fourtieth IAS Annual Meeting. Conference Record of the 2005*, vol. 4, Oct 2005, pp. 2849–2856 Vol. 4.

[22] G. Welch and G. Bishop, "An Introduction to the Kalman Filter," Department of Computer Science, University of North Carolina at Chapel Hill, Chapel Hill, NC 27599-3175, TR 95-041, July 2006.

[23] M. Abdullah, A. Yatim, C. Tan, and R. Saidur, "A review of maximum power point tracking algorithms for wind energy systems," *Renewable and Sustainable Energy Reviews*, vol. 16, no. 5, pp. 3220 – 3227, 2012. [Online]. Available: http://www.sciencedirect.com/science/article/pii/S1364032112001098

[24] N. Mohan, T. Underland, and W. Robbins, *Power Electronics: Converter, Applications and Design*, B. Zobrist, Ed. John Wiley & Sons, Inc., 2003.

[25] J. Persson, "Innovative Standstill Position Detection combined with sensorless control of synchronous motors," Ph.D. dissertation, Ecole Polytechnique Federale de Lausanne, 2005.

[26] T. Karvonen, "Stability of linear and non-linear Kalman filters," Master's thesis, University of Helsinki, 2014.

[27] *Rutland 913 Windcharger Owners Manual*, MARLEC, February 2013.

10. Appendices

Table 3 Measured and simulated rms values - Ampair turbine

Speed	250 RPM			
Load	7.4Ω	21Ω	43Ω	Max Error
Va measured (Vrms)	7.78	9.10	9.46	1.41%
Va simulated (Vrms)	7.67	9.04	9.37	
Ia measured (Arms)	1.06	0.42	0.22	9.09%
Ia simulated (Arms)	1.01	0.41	0.20	
Speed	500 RPM			
Load	7.4Ω	21Ω	43Ω	Max Error
Va measured (Vrms)	14.10	17.77	18.77	1.23%
Va simulated (Vrms)	14.13	17.99	18.81	
Ia measured (Arms)	1.92	0.82	0.42	4.76%
Ia simulated (Arms)	1.91	0.81	0.40	
Speed	1000 RPM			
Load	7.4Ω	21Ω	43Ω	Max Error
Va measured (Vrms)	21.97	33.40	36.71	2.18%
Va simulated (Vrms)	22.44	32.67	36.27	
Ia measured (Arms)	2.98	1.48	0.78	6.37%
Ia simulated (Arms)	3.17	1.56	0.80	

Table 4 Ampair wind turbine modelling - Datasheet ($*$), simulation (†) and experimental values (ψ)

Wind speed [m/s]	**5**	**8.26**	**10**	**12.09**	**14**	**20**	Max error
Power ($*$) [W]	16.3	45.9	65.3	79.4	89.0	102.0	54%
Power (†) [W]	8.8	41.3	63.3	78.3	88.1	102.2	17%
Power (ψ) [W]	7.5	43.5	64.4	82.5	91.0	104.3	
Cp ($*$)	0.315	0.197	0.159	0.109	0.076	0.031	55%
Cp (†)	0.170	0.177	0.153	0.107	0.077	0.031	22%
Cp (ψ)	0.139	0.186	0.151	0.112	0.080	0.031	
λ ($*$)	2.82	2.93	3.32	3.49	3.63	3.63	14%
λ (†)	3.29	3.26	3.34	3.49	3.60	3.74	2.1%
λ (ψ)	3.22	3.31	3.39	3.50	3.60	3.72	
I^2R losses (†) [W]	2.1	6.9	10.2	12.3	13.8	15.6	7.2%
I^2R losses (ψ) [W]	2.0	7.4	10.5	12.7	14.0	15.9	

Table 5 Rutland wind turbine modelling - Datasheet ($*$), simulation ($\dagger$) and experimental values (ψ)

Wind speed [m/s]	**5.85**	**7.45**	**8.37**	**9.3**	**11.64**	**12.96**	Max error
Power ($*$) [W]	21.42	32.4	42.84	45.66	89.1	109.5	22%
Power ($\dagger$) [W]	19.2	32.8	40.85	50.12	98.0	116.8	10%
Power (ψ) [W]	18.95	33.39	45.95	55.8	96.1	115.67	
Cp ($*$)	0.267	0.196	0.182	0.142	0.14	0.126	11%
Cp ($\dagger$)	0.241	0.199	0.179	0.156	0.156	0.134	8.6%
Cp (ψ)	0.237	0.202	0.196	0.174	0.152	0.133	
λ ($*$)	3.29	2.78	2.71	2.45	2.45	2.20	18%
λ ($\dagger$)	3.13	2.77	2.61	2.45	2.72	2.61	6.4%
λ (ψ)	3.21	2.78	2.79	2.69	2.70	2.51	
I^2R losses ($\dagger$) [W]	3.74	10.91	16.92	25.47	62.32	88.53	11%
I^2R losses (ψ) [W]	3.33	11.69	19.45	31.57	79.06	85.13	